7-1-2016

Intrinsic magnetic properties in R(Fe1−xCox)11TiZ(R=Yand Ce;Z=H,C,and N)

Liqin Ke
Ames Laboratory, liqinke@ameslab.gov

Duane D. Johnson
Iowa State University, ddj@iastate.edu

Intrinsic magnetic properties in R(Fe1−xCox)11TiZ(R=Yand Ce;Z=H,C,and N)

Abstract
To guide improved properties coincident with reduction of critical materials in permanent magnets, we investigate via density functional theory (DFT) the intrinsic magnetic properties of a promising system, R(Fe1−xCox)11TiZ with R=Y, Ce and interstitial doping (Z=H,C,N). The magnetization M, Curie temperature TC, and magnetocrystalline anisotropy energy K calculated in local density approximation to DFT agree well with measurements. Site-resolved contributions to K reveal that all three Fe sublattices promote uniaxial anisotropy in YFe11Ti, while competing anisotropy contributions exist in YCo11Ti. As observed in experiments on R(Fe1−xCox)11Ti, we find a complex nonmonotonic dependence of K on Co content and show that anisotropy variations are a collective effect of MAE contributions from all sites and cannot be solely explained by preferential site occupancy. With interstitial doping, calculated TC enhancements are in the sequence of N>C>H, with volume and chemical effects contributing to the enhancement. The uniaxial anisotropy of R(Fe1−xCox)11TiZ generally decreases with C and N; although, for R=Ce, C doping is found to greatly enhance it for a small range of 0.7

Disciplines
Metallurgy

Comments
This article is from Phys. Rev. B 94, 024423, doi:10.1103/PhysRevB.94.024423. Posted with permission.

Intrinsic magnetic properties in $R(Fe_{1-x}Co_x)_{11}TiZ$ (R = Y and Ce; Z = H, C, and N)

Liqin Ke[1,*] and Duane D. Johnson[1,2]

[1]*Ames Laboratory, US Department of Energy, Ames, Iowa 50011, USA*

[2]*Materials Science & Engineering, Iowa State University, Ames, Iowa 50011-2300, USA*

(Received 7 May 2016; revised manuscript received 6 July 2016; published 19 July 2016)

To guide improved properties coincident with reduction of critical materials in permanent magnets, we investigate via density functional theory (DFT) the intrinsic magnetic properties of a promising system, $R(Fe_{1-x}Co_x)_{11}TiZ$ with R = Y, Ce and interstitial doping (Z = H, C, N). The magnetization M, Curie temperature T_C, and magnetocrystalline anisotropy energy K calculated in local density approximation to DFT agree well with measurements. Site-resolved contributions to K reveal that all three Fe sublattices promote uniaxial anisotropy in $YFe_{11}Ti$, while competing anisotropy contributions exist in $YCo_{11}Ti$. As observed in experiments on $R(Fe_{1-x}Co_x)_{11}Ti$, we find a complex nonmonotonic dependence of K on Co content and show that anisotropy variations are a collective effect of MAE contributions from all sites and cannot be solely explained by preferential site occupancy. With interstitial doping, calculated T_C enhancements are in the sequence of N > C > H, with volume and chemical effects contributing to the enhancement. The uniaxial anisotropy of $R(Fe_{1-x}Co_x)_{11}TiZ$ generally decreases with C and N; although, for R = Ce, C doping is found to greatly enhance it for a small range of $0.7 < x < 0.9$.

DOI: 10.1103/PhysRevB.94.024423

I. INTRODUCTION

The search for new permanent magnets without critical materials has generated great interest in the magnetism community [1,2]. Developing $CeFe_{12}$-based rare-earth (R)-transition-metal (TM) intermetallics [3–7] is an important approach, considering the relative abundance of Ce among R elements and the large content of inexpensive Fe. To improve $CeFe_{11}Ti$ as a permanent magnet, it is desired to modify the compound to achieve the best possible intrinsic magnetic properties, such as magnetization M, Curie temperature T_C, and magnetocrystalline anisotropy energy (MAE) K. Both substitutional doping with Co [8] and interstitial doping with small elements of H, C, or N can strongly affect its magnetic properties. A theoretical understanding of intrinsic magnetic properties in this system and the effect of doping will help guide the experiments and help ascertain the best achievable permanent magnet properties.

Binary iron compounds of RFe_{12} do not form for any R elements unless a small amount of stabilizer elements are added, such as T = Ti, Si, V, Cr, Mo, or W [9]. Such $RFe_{12-z}T_z$ compounds are generally regarded as ternaries rather than pseudobinaries because the third element, T, atoms often have a very strong site preference and exclusively sit at one of three nonequivalent Fe sites [10]. Magnetization often decreases quickly with the increase of T composition and a minimum amount of Ti ($z = 0.7$) is needed to stabilize the structure, resulting in Ti compounds having better magnetic properties than others [11]. Prototype yttrium compounds are often studied to focus on the properties of the TM sublattices in the corresponding R-TM systems because yttrium can be regarded as a nonmagnetic, rare-earth element.

In comparison to other R-Fe systems [11,12], such as Y_2Fe_{17} and $Y_2Fe_{14}B$, Fe sublattices in 1-12 compounds have relative low magnetization due to a more compact structure, but at low temperatures a very high uniaxial MAE, e.g., $K = 2$ MJm^{-3} in $YFe_{11}Ti$ [8,13]. Curie temperatures are relatively low; M and K quickly decrease with increasing temperature [14–16]. $CeFe_{11}Ti$ has $T_C \approx 485$ K, and a low-temperature magnetization within a range of 17.4–20.2 μ_B/f.u., while $YFe_{11}Ti$ has a slightly larger M and T_C. At room temperature, $CeFe_{11}Ti$ has a larger K (1.3 MJm^{-3}) than $YFe_{11}Ti$ (0.89 MJm^{-3}). This may indicate that the Ce sublattice has a positive contribution to the uniaxial anisotropy [15].

The substitutional doping with Co is a common approach to improve T_C in R-Fe compounds [8]. Pure phase $R(Fe_{1-x}Co_x)_{11}Ti$ exists over the whole composition range for both R = Y and Ce [17]. The largest magnetization in $Y(Fe_{1-x}Co_x)_{11}Ti$ occurs at YFe_8Co_3Ti while the T_C increases continuously with Co composition until it reaches the maximum in $YCo_{11}Ti$ [18,19]. For Ce compounds, the maximum T_C is obtained in $CeFe_2Co_9Ti$ [17]. The dependence of MAE on the Co composition in $R(Fe_{1-x}Co_x)_{11}Ti$ is more intriguing and not understood. Although early experiments [8,14] suggested that $YCo_{11}Ti$ has a planar anisotropy, later experiments agreed that $YCo_{11}Ti$ has uniaxial anisotropy [17–23] but with a magnitude smaller than those of $YFe_{11}Ti$. For the intermediate Co composition, anisotropy changes from uniaxial to planar and then back to uniaxial with the increase of Co composition in both $Y(Fe_{1-x}Co_x)_{11}Ti$ and $Ce(Fe_{1-x}Co_x)_{11}Ti$ [17–23].

The interstitial doping with H [15], N [5,24,25], and C [26–28] can increase M and T_C and provide control of the magnitude and sign of the MAE constants in $RFe_{11}Ti$. Hydrogenation simultaneously increases all three intrinsic magnetic properties in $YFe_{11}Ti$, and enhancements are $\Delta M = 1\mu_B$/f.u. at 4.2 K, $\Delta T_C = 60$ K [16,29], and $\Delta K = 6.5\%$ [16], respectively. Insertion of larger C and N atoms has a much stronger effect on the enhancements of M and T_C [27,30]. Unfortunately, it is achieved at the expense of uniaxial anisotropy. In comparison with $YFe_{11}Ti$, enhancements of $\Delta M = 2.6\mu_B$/f.u. and $\Delta T_C = 154$ K were observed in $YFe_{11}TiC_{0.9}$, and $\Delta M = 2.7\mu_B$/f.u. and $\Delta T_C = 218$ K in $YFe_{11}TiN_{0.8}$. The MAE decreases

*liqinke@ameslab.gov

by $\Delta K = 0.6 \sim 0.7\ \mathrm{MJm}^{-3}$ in both compounds. Doping influences the MAE contributions from both TM sublattice and rare-earth atoms. It had been argued that the proximity of doping atoms to the rare-earth atoms in $R\mathrm{TiFe}_{11}\mathrm{N}_x$ may lead to drastic changes in the rare-earth sublattice anisotropy [25], and N doping often has an opposite effect on MAE as H doping [30]. For Ce compounds, a similar amount of T_C enhancement was obtained upon nitriding [5], and the effect of H doping is much smaller. Isnard *et al.* [15] found that not much change is observed upon H insertion either in the room temperature anisotropy or in saturation magnetization.

Other possible interstitial doping elements such as B, Si, or P atoms are much less favored to occupy the interstitial sites due to chemical or structural reasons [26]. In fact, interestingly, it has been found that the B atoms prefer to substitute for some of the Ti atoms and drive the Ti into the interstitial [31].

The nature of the Ce $4f$ state different Ce-TM compounds is often a controversial subject [32]. The anomalies in the lattice constants as well as the magnetic moment and Curie temperature have been interpreted as evidence of the mixed-valence (between Ce^{3+} and Ce^{4+}) behavior of the cerium ion. It is further complicated by the doping. Controversy remains on how Ce valence states are affected upon hydrogenation [15,33]. It also has been shown that Ce $4f$ states are itinerant and, as such, the standard localized $4f$ picture is not appropriate for systems such as CeCo_5 [34,35]. Moreover, in the $(\mathrm{Nd\text{-}Ce})_2\mathrm{Fe}_{14}\mathrm{B}$ system, the mixed valency of Ce has been shown to be due to local site volume and site chemistry effects [36]. In this paper the $4f$ states in Ce are treated as itinerant and included as valence states, and we found that magnetic properties calculated are in good agreement with experiments.

II. CALCULATION DETAILS

A. Crystal structure

$R\mathrm{Fe}_{11}\mathrm{Ti}$ has a body-center-tetragonal ThMn_{12}-type ($I4/mmm$ space group, no. 139) structure, which is closely related to the 1-5 and 2-17 R-TM structures [11]. The primitive unit cell contains one formula unit (f.u.). As shown in Fig. 1, R atoms occupy the $2a(4/mmm)$ site, while transition metal atoms are divided into three sublattices, $8i(m2m)$, $8j(m2m)$, and $8f(2/m)$, each of which has fourfold multiplicities. The $8j$ and $8f$ sites bear a great similarity in their local environments with respect to the distribution of coordinated atoms [37], whereas the $8i$ sites, often referred to as dumbbell sites, form -Fe-Fe-R- chains with R atoms along the basal axes, instead of the c axis, as in the 2-17 structure [38]. Ti atoms occupy nearly exclusively on the $8i$ sites, however, the distribution of Fe and Ti atoms within the $8i$ sites is disordered.

To calculate $R\mathrm{Fe}_{11}\mathrm{Ti}$, we replace one of four Fe($8i$) atoms with Ti in the primitive cell of $R\mathrm{Fe}_{12}$ and neglect the effect of the artificial Ti ordering introduced by using this unit cell. Although the $I4/mmm$ symmetry is lowered by Ti substitution or the spin-orbit coupling (SOC) in the anisotropy calculation, we still use the notations of $8j$, $8i$, and $8f$ sites for simplicity.

For Co doping, Mössbauer spectroscopy found that Co atoms preferentially occupy the $8f$ sites in $\mathrm{Y(Fe}_{1-x}\mathrm{Co}_x)_{11}\mathrm{Ti}$ [39], while the high-resolution neutron powder diffraction experiments concluded that Co atoms preferentially occupy sites in the sequence of $8j > 8f > 8i$ [40]. For interstitial H, C, and N doping, neutron scattering has shown that dopants prefer to occupy the larger octahedral $2b$ interstitial sites [15,25], which have the shortest distance from the rare-earth sites among all empty interstitial sites. In all our calculations, we also assume that H, C, or N atom occupies the $2b$ sites.

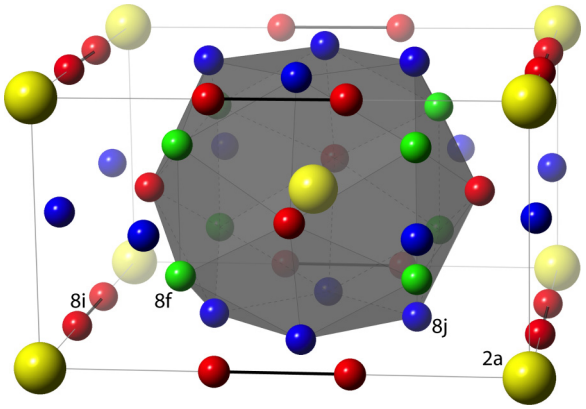

FIG. 1. Schematic representation of the crystal structures of $R\mathrm{Fe}_{11}\mathrm{Ti}$. $R(2a)$ atoms are indicated with larger spheres in yellow color. Three transition metal sublattices $8i$, $8j$, and $8f$ are in red, blue, and green, respectively. Each R atom has four nearest $8i$, eight nearest $8j$, and $8f$ neighbor atoms. Among three TM sites, the $8i$ site has the shortest distance from the R atom. Interstitial sites $2b$ (not shown) are halfway between two R atoms along the c axis and coordinated by an octahedron of two R and four Fe($8j$) sites.

B. Computational methods

Most magnetic properties were calculated using a standard linear muffin-tin orbital (LMTO) basis set [41] generalized to full potentials [42]. This scheme employs generalized Hankel functions as the envelope functions. For MAE calculation, the SOC was included through the force theorem [43]. The MAE is defined below as $K = E_{110} - E_{001}$, where E_{001} and E_{110} are the summation of band energies for the magnetization being oriented along the [001] and [110] directions, respectively. Positive (negative) K corresponds to uniaxial (planar) anisotropy. It should be noted that, due to the presence of Ti in the primitive cell, the two basal axes become inequivalent, with -Ti-Fe-R- chains along the [100] direction and -Fe-Fe-R- chains along the [010] direction. E_{100} and E_{010} become different, which is an artifact introduced by using the small primitive cell and artificial ordering of Ti within the $8i$ sublattice.

We found that the [100] direction is harder than the [010] in $\mathrm{YFe}_{11}\mathrm{Ti}$, and vice versa in $\mathrm{YCo}_{11}\mathrm{Ti}$. E_{110} is usually about the average of E_{100} and E_{010}. Thus, we use [110] as the reference direction for the basal plane. A $16 \times 16 \times 16\,k$-point mesh is used for MAE calculations to ensure sufficient convergence; MAE in $\mathrm{YFe}_{11}\mathrm{Ti}$ changed by less than 3% when a denser $32 \times 32 \times 32$ mesh was employed. To decompose the MAE, we evaluate the on-site SOC matrix element $\langle V_{\mathrm{so}} \rangle$ and the corresponding anisotropy $K_{\mathrm{so}} = \frac{1}{2}\langle V_{\mathrm{so}} \rangle_{110} - \frac{1}{2}\langle V_{\mathrm{so}} \rangle_{001}$. Unlike MAE, K_{so} can be easily decomposed into sites, spins, and orbital pairs. According to second-order perturbation

theory [44,45],

$$K \approx \sum_i K_{\rm so}(i), \tag{1}$$

where i indicates atomic sites. Equation (1) holds true for all compounds that we investigated in this paper. Hence, we use $K_{\rm so}(i)$ to represent the site-resolved MAE. For simplicity, we write it as $K(i)$.

Exchange coupling parameters J_{ij} are calculated using a static linear-response approach implemented in a Green's function (GF) LMTO method, simplified using the atomic sphere approximation (ASA) to the potential and density [46,47]. The scalar-relativistic Hamiltonian was used so SOC is not included, although it is a small perturbation on J_{ij}'s. In the basis set, s,p,d,f orbitals are included for Ce, Y, Fe, and Co atoms, and s,p orbitals are included for H, C, and N atoms. Exchange parameters $J_{ij}(\mathbf{q})$ are calculated using a 16^3 k-point mesh, and $J_{ij}(\mathbf{R})$ can be obtained by a subsequent Fourier transforming. $T_{\rm C}$ is estimated in the mean-field approximation (MFA) or random-phase approximation (RPA). See Ref. [46] for details of the methods to calculate $T_{\rm C}$.

For all magnetic property calculations, the effective one-electron potential was obtained within the local density approximation (LDA) to DFT using the parametrization of von Barth and Hedin [48]. However, with the functional of Perdew, Becke, and Ernzerhof (PBE) being better at structural relaxation for most of the solids containing 3d elements [49], we use it to fully relax the lattice constants and internal atomic positions in a fast plane-wave method, as implemented within the Vienna *ab initio* simulation package (VASP) [50,51]. The nuclei and core electrons were described by the projector augmented wave (PAW) potential [52] and the wave functions of valence electrons were expanded in a plane-wave basis set with a cutoff energy of up to 520 eV. All relaxed structures are then verified in FP-LMTO before the magnetic property calculations are performed.

III. RESULTS AND DISCUSSION

A. Structure

Lattice constants and volumes are listed in Table I; the calculated lattice constants are in good agreement with experiments. The strong Ti site preference on the 8i site [3,15,54] had been interpreted in terms of atomic volume, coordination number, and enthalpy. It had been argued that enthalpy associated with R and Ti, V, or Mo atoms are positive and 8i sites have the smallest contact area with R atoms. To identify quantitatively the site-preference effect, we calculated the total energy of $CeFe_{11}Ti$ with one Ti atom occupying at the 8i, 8j, or 8f sites, respectively, in the 13-atom primitive cell. The lowest-energy structure is the one with Ti atoms on the 8i site. Energies are higher by 42 meV/atom and 60 meV/atom with Ti atom being on the 8j and 8f sites, respectively. Hence, Ti atom should have a strong preference to occupy the 8i sites, as observed in the experiments.

In comparison to the hypothetical 1-12 compounds, the replacement of Fe or Co atoms with Ti increases volume by 1% or 2%, respectively. Experimentally, H doping slightly increases the volume by 1% in $YFe_{11}TiH$, which is not observed in our calculation. The calculated volume of $CeFe_{11}TiH$ is 0.82% larger than $CeFe_{11}Ti$. Calculations show that carbonizing and nitriding have a larger effect on volume expansion than hydrogenation and volume expansion is larger in Ce compounds than in Y compounds, both of which agree with experiments.

TABLE I. Calculated and measured (Expt.) values for the lattice parameters and volume are listed for various compounds.

Compounds	a[a] (Å)	c (Å)	V (Å^3)	$\Delta V/V$	Ref.
$YFe_{11}Ti$ (Expt.)	8.480	4.771	343.08		[53]
$YFe_{11}Ti$	8.472	4.720	338.78	0	
YFe_{12}	8.447	4.695	334.94	−1.1	
$YFe_{11}TiH$	8.457	4.732	338.43	−0.10	
$YFe_{11}TiC$	8.517	4.834	350.67	3.51	
$YFe_{11}TiN$	8.563	4.791	351.31	3.70	
$YCo_{11}Ti$ (Expt.)	8.367	4.712	329.87		[54]
$YCo_{11}Ti$	8.328	4.673	324.08	0	
YCo_{12}	8.268	4.655	318.21	−1.81	
$YCo_{11}TiH$	8.343	4.688	326.30	0.68	
$YCo_{11}TiC$	8.396	4.767	336.08	3.70	
$YCo_{11}TiN$	8.436	4.716	335.59	3.55	
$CeFe_{11}Ti$ (Expt.)	8.539	4.780	348.53		[15]
$CeFe_{11}Ti$	8.524	4.670	339.35	0	
$CeFe_{12}$	8.504	4.648	336.12	−0.95	
$CeFe_{11}TiH$	8.498	4.738	342.13	0.82	
$CeFe_{11}TiC$	8.501	4.891	353.45	4.16	
$CeFe_{11}TiN$	8.570	4.809	353.17	4.07	
$CeCo_{11}Ti$ (Expt.)	8.380	4.724	331.74		[17]
$CeCo_{11}Ti$	8.360	4.657	325.46	0	
$CeCo_{12}$	8.291	4.648	319.51	−1.82	
$CeCo_{11}TiH$	8.359	4.694	327.94	0.76	
$CeCo_{11}TiC$	8.383	4.811	338.07	3.87	
$CeCo_{11}TiN$	8.442	4.735	337.44	3.68	

[a]Except for the hypothetical 1-12 compounds, Ti substitution in the 13-atom cell breaks the symmetry of $CeFe_{12}$, and lattice parameters a and b become nonequivalent. The listed calculated a is an average of a and b of the unit cell used in the calculation.

The total density of states of $YFe_{11}Ti$ and $YFe_{11}TiN$ compares reasonably well with previously reported LMTO-ASA calculations [6]. Figure 2 shows the scalar-relativistic partial density of states (PDOS) projected on individual elements in $YFe_{11}Ti$, $YFe_{11}TiH$, $YFe_{11}TiC$, and $YFe_{11}TiN$. The Fe PDOS are averaged over 11 Fe atoms. The interstitial doping elements on 2b sites hybridizes with neighboring R and Fe(8j) atoms. H-s states hybridize with neighboring Y and Fe(8j) atoms at around −7 eV below the Fermi level in $YFe_{11}TiH$. The C-p and N-p states have larger energy dispersion in $YFe_{11}TiC$ and $YFe_{11}TiN$, respectively. The Fe states hybridized with interstitial elements, as shown in Fig. 2, are mostly from four (8j) out of 11 Fe sites. Fe(8f) sites are the furthest away from the interstitial 2b sites and their hybridization with doping elements are negligible. The Ce compounds have large f states above the Fermi level and share lots of similar PDOS features with the corresponding Y compounds below the Fermi level.

B. Magnetization, exchange couplings, and $T_{\rm C}$

Intrinsic magnetic properties of each compound are listed in Table II. Experimental magnetization and anisotropy values

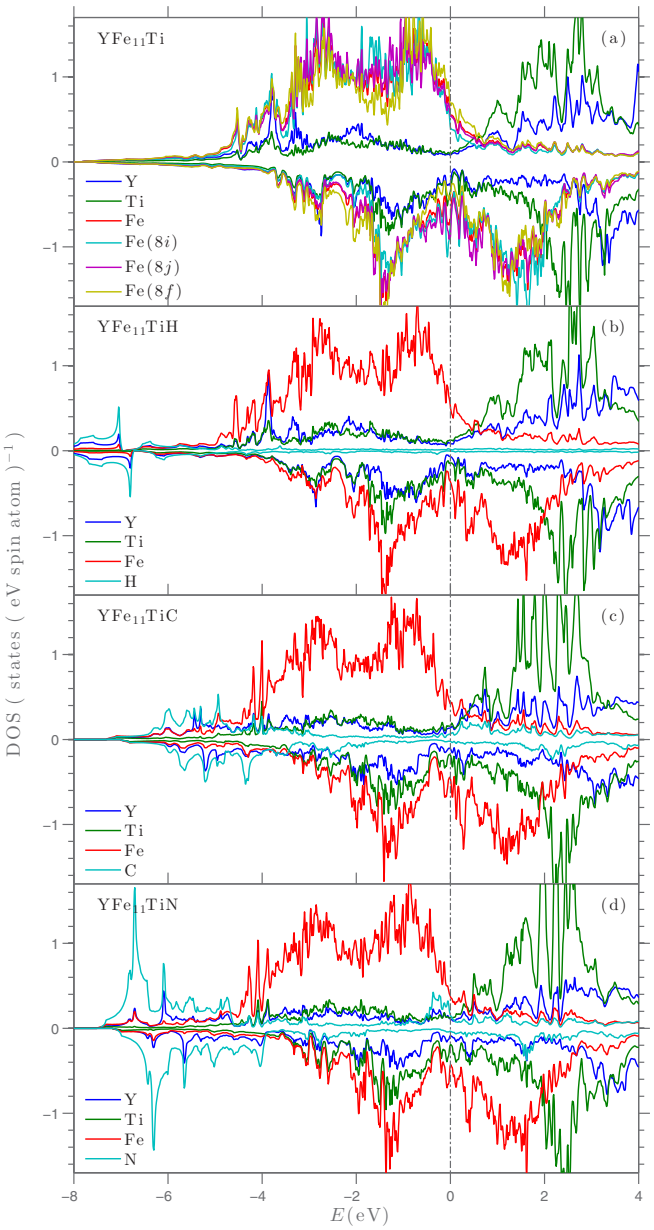

FIG. 2. Atom- and spin-projected partial densities of states (DOS) in (a) $YFe_{11}Ti$, (b) $YFe_{11}TiH$, (c) $YFe_{11}TiC$, and (d) $YFe_{11}TiN$ within the LDA and no SOC. For $YFe_{11}Ti$, the Fe DOS are further resolved by averaging states projected on $8i$, $8j$, and $8f$ sites. Majority spin (positive values) and minority spin (negative values) DOS are shown separately. Fermi energy E_F is at 0 eV.

vary. The calculated magnetizations in $YFe_{11}Ti$, $YCo_{11}Ti$, and $CeFe_{11}Ti$ compare well with experiments. For $CeCo_{11}Ti$, only a limited number of studies had been reported, and the calculated magnetization is larger than experimental ones. Ti spin moments couple antiparallel to those of Fe and Co sublattices, which is typical for the light $3d$ and $4d$ elements [56]. In $CeFe_{11}Ti$, the Ce spin moments antiferromagnetically couple with the TM sublattice as expected [57]. Ce has a spin moment $m_s \approx -0.7\ \mu_B$ and an orbital moment $m_l \approx 0.3\ \mu_B$ with the opposite sign, which reflects Hund's third rule. The calculated Fe spin moments on the individual sublattice have the magnitude in the sequence of $m_s(8i) > m_s(8j) > m_s(8f)$, which agrees with previous experiments and calculations [58]. The dumbbell $8i$ sites have larger spin magnetic moments because of the relative larger surrounding empty volume and smaller atomic coordination number. The orbital magnetic moments calculated are larger in the Co-rich compounds than the Fe-rich compounds. MFA overestimated T_C by about 200 K in Fe compounds and about 50–100 K in Co compounds, respectively. RPA gives lower T_C values, e.g., 489 K in $YFe_{11}Ti$, and 461 K in $CeFe_{11}Ti$, respectively. The experimental T_C falls between the MFA and RPA values, and is much closer to the latter.

Ti additions decrease the magnetization by 20% in $RFe_{11}Ti$ and $RCo_{11}Ti$ relative to their 1-12 hypothetical counterparts. The magnetization reduction is not only due to the replacement of ferromagnetic Fe by antiferromagnetic Ti atoms (spin moment $-0.54\ \mu_B$) but also the suppression of the ferromagnetism on the neighboring Fe sublattices. This is a common effect of doping early $3d$ or $4d$ elements on the Fe or Co sublattice [56]. On the other hand, the addition of the Ti atom barely affects the Ce moment. Interestingly, although magnetization decreased by 20% upon the Ti addition, the calculated T_C is even slightly higher in $YFe_{11}Ti$ than in YFe_{12}. This is somewhat reflected in the experiments, in which no obvious T_C dependence on Ti composition was observed in $YFe_{11-z}Ti_z$ over the homogeneous 1-12 phase composition range, $0.7 \leqslant z \leqslant 1.25$ [11].

To understand this phenomenon, we investigated the effective exchange coupling parameters $J_0(i) = \sum_j' J_{ij}$ and compare J_0 values in YFe_{12} and $YFe_{11}Ti$. With Ti replacing one Fe atom, J_0 values increase for all sites except the pair of Ti-Fe dumbbell sites. The overall J_0 and the mean-field T_C increase. The site-resolved effective exchange parameters $J_0(i)$ for various compounds are listed in Table II.

Figure 3 shows the magnetization as a function of the Co composition in $YFe_{11}Ti$, with similar behavior to the Slater-Pauling curve. The maximum magnetization occurs at $x = 0.2$, while in experiments it is at $x = 0.3$ [19]. Similarly, for $Ce(Fe_{1-x}Co_x)_{11}Ti$, the experimental maximum magnetization occurs at $x = 0.1$–0.15 [55]. As shown in Table II, the $RCo_{11}Ti$ compounds have much larger T_C than the corresponding $RFe_{11}Ti$ compounds, which agrees with experiments [17].

All interstitial doping increases M and T_C in $YFe_{11}Ti$ and $CeFe_{11}Ti$, and nitriding has the strongest effect. With H, C, and N doping, the calculated Curie temperature in $YFe_{11}Ti$ increases by 51, 157, and 211 K, respectively, which is consistent with experiments. J_0 values on all three TM sublattices increase with interstitial doping. Although DFT underestimates the volume expansion with H doping, the calculated ΔT_C is only slightly smaller than the experimental value. The calculated ΔT_C is larger with N doping than C doping, while their calculated volume expansions are similar. This indicates that both volume and chemical effects are important for the T_C enhancement. To estimate qualitatively the relative magnitudes of the two effects, we calculate the T_C of several hypothetical compounds related to $YFe_{11}TiN$ by removing the N atom in the unit cell or replacing it with H or C atoms, respectively. The calculated ΔT_C of those structures relative to $YFe_{11}Ti$ are 53, 80, and 169 K, respectively. Obviously, both volume and chemical effects contribute to

TABLE II. Calculated spin M_s, orbital M_l, and total M_t magnetization, exchanges J_0, Curie temperature T_C estimated in the mean-field approximation, and magnetocrystalline anisotropy K in various compounds. Unless specified, experimental magnetization and anisotropy K values from previous studies were measured or evaluated for low temperature (<5 K).

Compound	M_s	M_l	M_t	J_0 (meV)					T_C	ΔT_C	K		Ref.
	($\frac{\mu_B}{\text{f.u.}}$)			8i (Ti)	8i	8j	8f	Y	K		($\frac{\text{meV}}{\text{f.u.}}$)	($\frac{\text{MJ}}{\text{m}^3}$)	
YFe_{12}	24.20	0.61	24.81		7.57	4.91	5.10	1.34	689	−38	1.40	1.34	
$YFe_{11}Ti$ (Expt.)			19–20.6						524–538			2.0	[8,11,16,19,27]
$YFe_{11}Ti$	19.75	0.60	20.35	5.29	7.17	6.70	6.61	1.43	727	0	1.93	1.83	
$YFe_{11}TiH$	19.92	0.54	20.46	4.99	7.63	7.46	7.57	1.40	778	51	2.07	1.96	
$YFe_{11}TiC$	20.64	0.55	21.19	5.51	8.58	8.83	8.66	1.67	884	157	0.95	0.87	
$YFe_{11}TiN$	22.11	0.57	22.68	5.44	9.36	8.91	9.29	1.30	938	211	1.80	1.65	
$YCo_{11}Ti$ (Expt.)			14.2–15.7						1020–1050			0.75[a]	[18,19]
$YCo_{11}Ti$	14.42	0.82	15.24	3.93	10.50	10.13	11.13	1.45	1091	364	0.94	0.93	
YCo_{12}	18.42	0.90	19.32		12.52	13.12	13.84	1.66	1374	647	0.48	0.48	
$CeFe_{12}$	24.02	0.78	24.80		8.69	7.33	6.12	1.75	806	131	1.77	1.69	
$CeFe_{11}Ti$ (Expt.)			17.4–20.2						482–487			1.3[a]–2.0[a]	[5,15,17,18,55]
$CeFe_{11}Ti$	19.19	0.72	19.91	4.69	6.26	7.04	5.95	2.16	675	0	2.09	1.98	
$CeFe_{11}TiH$	20.24	0.77	21.01	4.67	6.87	7.42	7.04	2.30	736	61	2.03	1.90	
$CeFe_{11}TiC$	19.84	0.73	20.57	5.45	9.86	8.62	8.62	3.44	908	233	1.09	0.99	
$CeFe_{11}TiN$	21.48	0.67	22.15	5.51	9.09	8.53	8.99	1.09	905	230	1.78	1.62	
$CeCo_{11}Ti$ (Expt.)			10.9–12.53[a]						920–937		Axial		[17,18]
$CeCo_{11}Ti$	13.77	1.32	15.09	4.07	10.40	9.38	10.94	3.76	1044	369	1.29	1.23	
$CeCo_{12}$	17.35	1.36	18.71		12.03	12.29	12.97	3.80	1286	611	1.24	1.24	

[a]Measured at room temperature.

the T_C enhancement, and the chemical effects of interstitial elements are in the sequence of N > C > H.

C. MAE in $R(Fe_{1-x}Co_x)_{11}Ti$

As listed in Table II, both $YFe_{11}Ti$ and $YCo_{11}Ti$ have uniaxial anisotropy. Calculated MAE in $YFe_{11}Ti$ is in good agreement with the experimental value. $CeFe_{11}Ti$ has a slightly larger MAE than $YFe_{11}Ti$ as found in experiments [15,32]. The PBE functional (not shown) gives a smaller MAE than LDA in $YFe_{11}Ti$ and $CeFe_{11}Ti$.

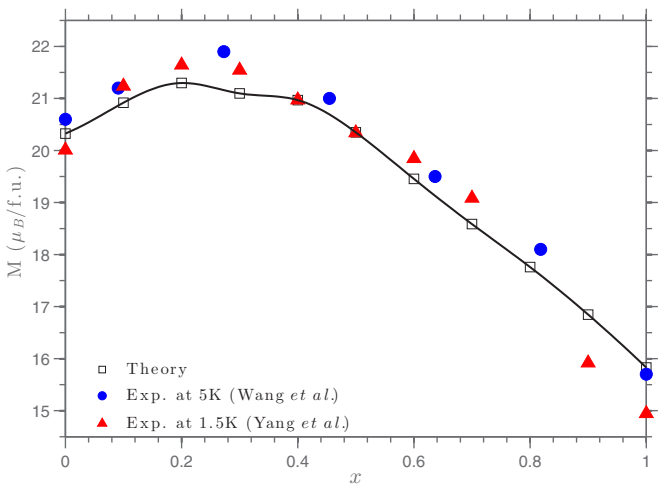

FIG. 3. Comparison of measured and calculated (squares) M versus Co content in $Y(Fe_{1-x}Co_x)_{11}Ti$. Experimental data are from Wang *et al.* [19] at 5 K (circles) and Yang *et al.* [8] at 1.5 K (triangles).

The Fe sublattice anisotropy may have a strong dependence on the composition of stabilizer atoms [14]. To understand how Ti affects the magnetic anisotropy and the origin of the nonmonotonic dependence of MAE on Co composition, we resolved MAE into sites by evaluating the matrix element of the on-site SOC energy [44,45]. For intermediate Co composition, we investigate the MAE in YFe_7Co_4Ti and YFe_3Co_8Ti. We calculated the formation energy relative to $YFe_{11}Ti$ and $YCo_{11}Ti$ and found that YFe_7Co_4Ti has a formation energy $E_{\text{fmn}} = -34$ meV/atom with four Co atoms on the 8j sites and $E_{\text{fmn}} = -28$ meV/atom with four Co atoms on the 8f sites. Both values are lower than $E_{\text{fmn}}=-10$ meV/atom, the formation energy of YFe_8Co_3Ti with all three Co atoms being on the 8i sites. Hence, the site preference of Co atoms is 8j > 8f > 8i, which agrees with the neutron scattering experiments [40]. For YFe_3Co_8Ti, we occupy another four Co atoms on the 8f sites and the corresponding formation energy is −31 meV/atom.

Figure 4 shows the total MAE values and their sublattice-resolved components, in YFe_{12}, YFe_7Co_4Ti, YFe_3Co_8Ti, and $YCo_{11}Ti$. Obviously, Eq. (1) is well satisfied in all compounds and K_{so} presents well the site-resolved MAE. The Y sublattice has a negligible contribution to anisotropy, as expected for a weakly magnetic atom, because the spin-parallel components of MAE contribution cancel out the spin-flip ones [45]. Sublattice-resolved MAE contributions in YFe_{12} shows $K(8j) > K(8i) > 0 > K(8f)$, which agrees with the previous estimation in sign but differs in the order [11]. Considering Fe(8i) sites have positive contributions to the uniaxial anisotropy in YFe_{12}, one may expect that replacing Fe atoms by the Ti atoms on the 8i site would decrease MAE. Interestingly, we found that $YFe_{11}Ti$ has even larger uniaxial anisotropy than YFe_{12}. Anisotropies of all three sublattices

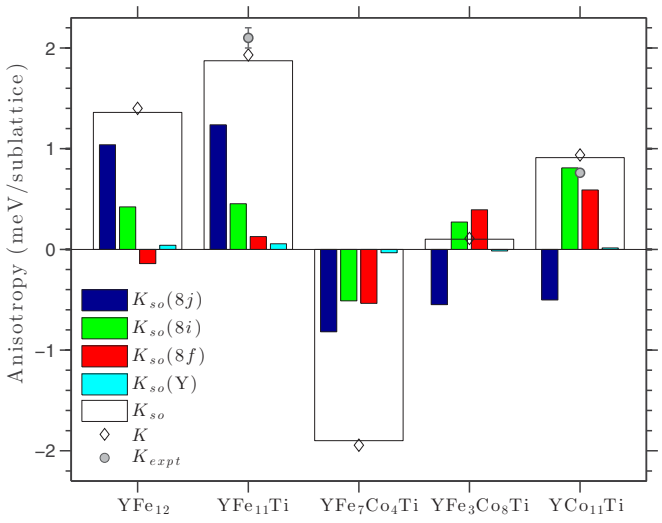

FIG. 4. Total and sublattice-resolved K_{so} in $YFe_{11}Ti$, YFe_7Co_4Ti, YFe_3Co_8Ti, and $YCo_{11}Ti$. Calculated K and measured K_{expt} values are also compared. Experimental values were from Refs. [29] and [18], measured at 4.2 K for $YFe_{11}Ti$ and 293 K for $YCo_{11}Ti$, respectively. In calculations, we assume that all four Co occupy the $8j$ sites in YFe_7Co_4Ti while all eight Co occupy the $8j$ and $8f$ sites in YFe_3Co_8Ti.

become more uniaxial and $K(8j) > K(8i) > K(8f) > 0$ in $YFe_{11}Ti$, which indicates that the introduction of Ti atoms modifies the electronic structure of neighboring sites and enhances their contribution to uniaxial anisotropy. Similarly, other compounds, such as $YCo_{11}Ti$, $CeFe_{11}Ti$, and $CeCo_{11}Ti$, are also found to have MAE values larger than or similar to their corresponding hypothetical 1-12 counterparts.

The dependence of MAE on the Co composition is nonmonotonic and also found in other R-TM systems [59]. As shown in Fig. 4, the calculated MAE reproduce the trend observed in experiment. For intermediate Co compositions, YFe_7Co_4Ti compound has planar anisotropy while YFe_3Co_8Ti compound has a very small uniaxial anisotropy. The $8j$ sublattice is the major contributor to the uniaxial anisotropy in $YFe_{11}Ti$. With all four $8j$ Fe atoms being replaced by Co atoms in YFe_7Co_4Ti, $K(8j)$ becomes very negative. Moreover, $K(8i)$ and $K(8f)$ are also strongly affected and become negative. Further Co doping on $8f$ sites changes $K(8i)$ and $K(8f)$ back to positive in YFe_3Co_8Ti. Finally, in $YCo_{11}Ti$ both $K(8i)$ and $K(8f)$ increase and $K(8j)$ becomes less planar, and we have $K(8i) > K(8f) > 0 > K(8j)$.

The nonmonotonic composition dependence is often interpreted by preferential site occupancy [59], however, such an explanation is an oversimplification for a metallic system such as $Y(Fe_{1-x}Co_x)_{11}Ti$. The MAE contributions from each TM sublattice may depend on the detailed band structure around the Fermi energy. The doping of Co on particular sites unavoidably affects the electronic structure of neighboring TM sublattices due to the hybridization between them, which changes the MAE contribution from neighboring sites. Obviously, as shown in Fig. 4, with a sizable amount of Co doping, the variation of anisotropy is a collective effect instead of a sole contribution from the doping sites.

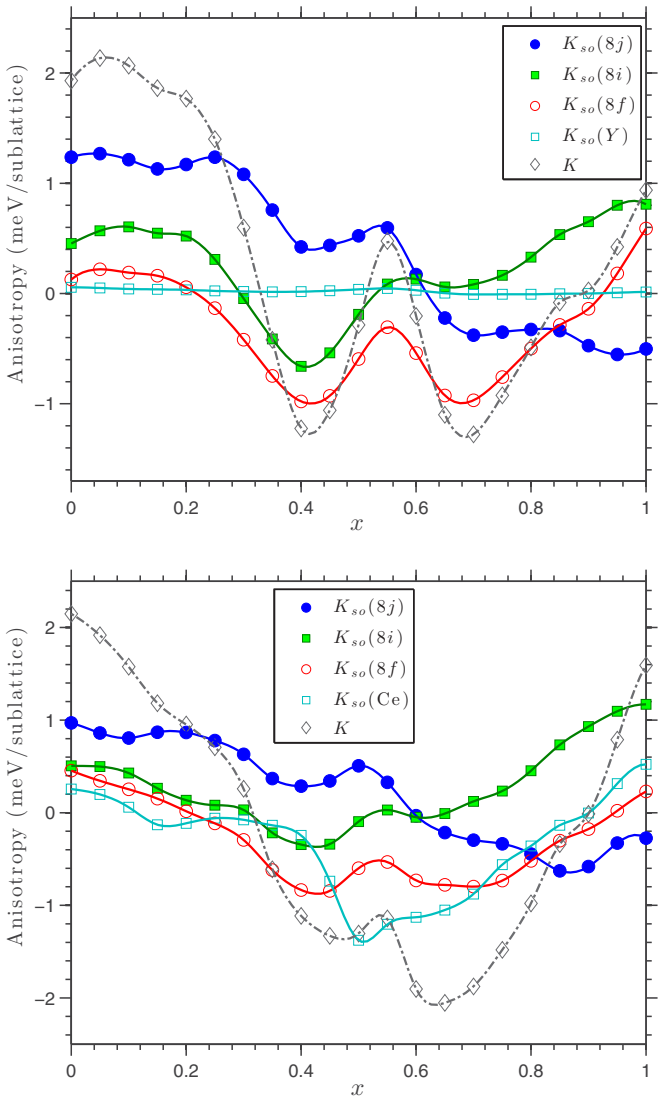

FIG. 5. K and sublattice-resolved K_{so} in Y-based (top) and Ce-based (bottom) $R(Fe_{1-x}Co_x)_{11}Ti$.

Among three TM sublattices, the dumbbell $8i$ sites have the largest contribution to the uniaxial anisotropy in $YCo_{11}Ti$, which we found also true in $CeCo_{11}Ti$, and hypothetical YCo_{12} and $CeCo_{12}$. It is interesting to compare the MAE contributions from Co sublattices in RCo_{12} and R_2Co_{17}, in which the dumbbell Co sites have the most negative contribution to the uniaxial anisotropy [38]. In both cases, the moments of the dumbbell sites prefer to be perpendicular to the dumbbell bonds, which are along different directions in two structures, i.e., basal axes in the 1-12 structure and c axis in the 2-17 structure. As a result, dumbbell Co sites have MAE contributions of opposite sign in two structures.

In a real sample, Co likely also partially occupies the $8j$ and $8f$ sites instead of exclusively only the $8j$ site. We investigate the scenario at the other extreme by assuming Co occupies the three TM sublattices with equal probability and calculate composition dependence of MAE using the virtual crystal approximation (VCA). Interestingly, the nonmonotonic behavior is also observed as shown in Fig. 5. The easy

direction changes from uniaxial to in-plane and then back to uniaxial. The variations of each individual TM sublattice share a similarity with the trend shown in Fig. 4. With increasing of x in $Y(Fe_{1-x}Co_x)_{11}Ti$, $K(8j)$ decreases and becomes negative while $K(8i)$ and $K(8f)$ become negative for the intermediate Co composition and then change back to positive at the Co-rich end. Thus, the nonmonotonic behavior is confirmed with or without considering preferential occupancy. The spin-reorientation transition [21] from axis to in-plane occurs in $Y(Fe_{1-x}Co_x)_{11}Ti$ but not pure $YFe_{11}Ti$ [21], which may relate to the fact that the competing anisotropies between three TM sublattices exist in $Y(Fe_{1-x}Co_x)_{11}Ti$ while all three TM sublattices support the uniaxial anisotropy in $YFe_{11}Ti$. As shown in Fig. 5 (top), MAE in $Y(Fe_{1-x}Co_x)_{11}Ti$ barely changes or even slightly increases with a very small Co composition. A similar feature had been observed experimentally [60]. It is caused by the partial occupation of Co on $8f$ sites in $YFe_{11}Ti$. We found that replacing Fe atoms in $YFe_{11}Ti$ with Co atoms on the $8f$ sites increases the MAE.

It is commonly assumed that the MAE contributions from the TM sublattices are similar in R-TM compounds with different R, and such contributions are often estimated experimentally from measurements on corresponding yttrium compounds [12]. As shown in Fig. 5, MAE contributions from TM sublattices in $YFe_{11}Ti$ and $CeFe_{11}Ti$ are similar but not identical. All three TM sublattices have positive contributions to the uniaxial anisotropy and $K(8j) > K(8i) > K(8f) > 0$. However, magnitudes of each sublattice differ in two compounds, which suggests that the hybridization TM sites have with different R atoms affects their contributions to the MAE. Unlike the Y sublattice in $YFe_{11}Ti$, Ce provides a positive contribution to the uniaxial anisotropy in $CeFe_{11}Ti$.

D. Effect of interstitial doping

Interstitial doping with N, C, and H affects the MAE from both the Fe and R sublattices [30]. As shown in Table II, H doping barely changes or slightly increases the uniaxial anisotropy in $YFe_{11}Ti$ and $CeFe_{11}Ti$ while carbonizing and nitriding weaken the uniaxial anisotropy, which agrees with experiments [5,27]. Simultaneous substitutional Co doping and interstitial doping with H, C, or N is of interest. Although the uniaxial anisotropy may not improve that much at the low temperature, the effect could be more significant at room temperature. For example, upon hydrogenation, a significant increase of K_1 with a factor 1.8 was observed in YFe_9Co_2Ti at room temperature [60].

To our knowledge, simultaneous doping of Co and interstitial elements C and N atoms is not well studied. We calculated the MAE dependence on Co compositions in $Ce(Fe_{1-x}Co_x)_{11}TiZ$ with $Z =$ H, C, and N, and results are shown in Fig. 6. The site preference of Co is not considered and VCA is used. The maximum of uniaxial anisotropy in $Y(Fe_{1-x}Co_x)_{11}TiH$ is obtained at $x = 0.1$ while experiments found the maximum at YFe_9Co_2TiH [60]. For the Fe-rich $CeCo_{11}TiZ$, only H doping slightly increases the MAE, while C and N quickly decrease uniaxial anisotropy. For $Y(Fe_{1-x}Co_x)_{11}TiZ$, it is unlikely we can have better uniaxial anisotropy (at least at low temperature) over the whole range of Co composition. Interestingly, for Co-rich

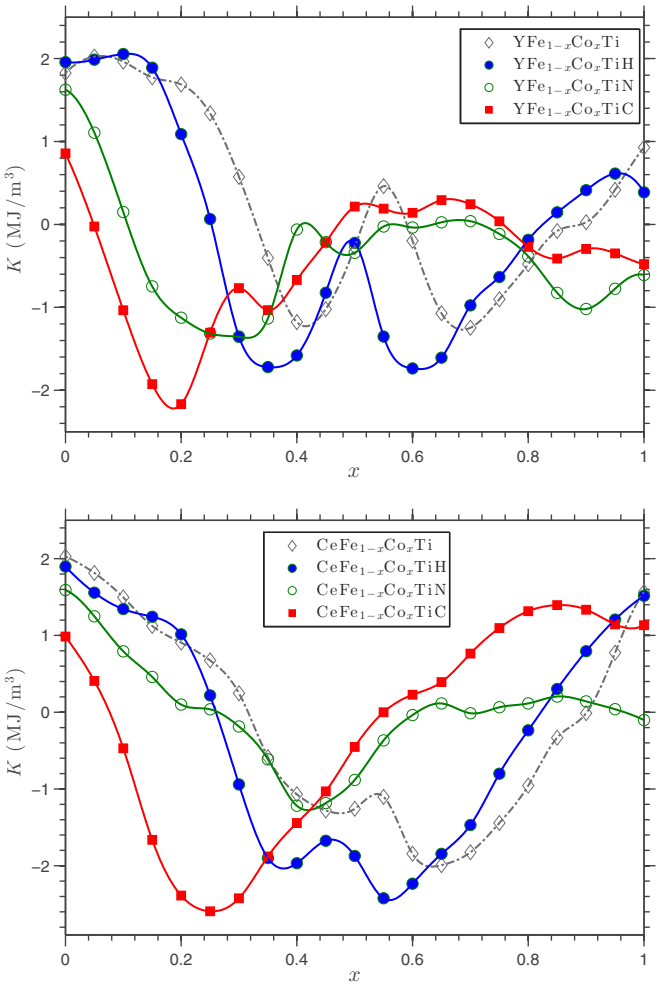

FIG. 6. K versus Co content in $R(Fe_{1-x}Co_x)_{11}TiZ$ with $R =$ Y (top) and $R =$ Ce (bottom), with and without $Z =$ H, C, and N.

$Ce(Fe_{1-x}Co_x)_{11}TiZ$, interstitial C doping significantly improves the uniaxial anisotropy in $Ce(Fe_{1-x}Co_x)_{11}TiZ$ for $0.7 < x < 0.9$. Considering the relative high Curie temperature on the Co-rich end, it has an attractive combination of all three intrinsic magnetic properties, M, J, and K, for permanent magnet application.

IV. CONCLUSION

Using DFT methods, the intrinsic magnetic properties of $RFe_{11}Ti$-related systems were investigated for the effects of substitutional alloying with Co and interstitial doping with H, C, and N. All properties and trends were well described within the local density approximation to DFT. In comparison to the hypothetical YFe_{12}, Ti quickly decreases the magnetization and increases the uniaxial magnetic anisotropy in $YFe_{11}Ti$. The calculated Co site preference is $8j > 8f > 8i$ in $Y(Fe_{1-x}Co_x)_{11}Ti$ with $x < 0.4$, in agreement with neutron experiments. The enhancement of M and T_C due to Co doping and interstitial doping are in good agreement with experiments.

Compared with $YFe_{11}Ti$, the calculated T_C increases by 51, 157, and 211K in $YFe_{11}TiZ$ with $Z =$ H, C, and N, respectively, with both volume and chemical effects con-

tributing to the enhancement. We found that all three Fe sublattices promote uniaxial anisotropy in the sequence of $K(8j) > K(8i) > K(8f) > 0$ in $YFe_{11}Ti$, while competing contributions give $K(8i) > K(8f) > 0 > K(8j)$ in $YCo_{11}Ti$. For intermediate Co composition, we confirm that the easy direction changes with increasing Co content from uniaxial to in-plane and then back to uniaxial. Substitutional doping affects the MAE contributions from neighboring sites, and the nonmonotonic composition dependence of anisotropy is a collective effect, which cannot be solely explained by preferential occupancy. The Ce sublattice promotes the uniaxial anisotropy in $CeFe_{11}Ti$ and $CeCo_{11}Ti$. Interstitial C doping significantly increases the uniaxial anisotropy in $Ce(Fe_{1-x}Co_x)_{11}Ti$ for $0.7 < x < 0.9$, which may provide the best combination of all three intrinsic magnetic properties for permanent applications.

ACKNOWLEDGMENTS

We thank B. Harmon, A. Alam, C. Zhou, and R. W. McCallum for helpful discussions. This work was supported by the U.S. Department of Energy ARPA-E (REACT 0472-1526). Ames Laboratory is operated for the U.S. DOE by Iowa State University under Contract No. DE-AC02-07CH11358.

[1] R. McCallum, L. Lewis, R. Skomski, M. Kramer, and I. Anderson, Annu. Rev. Mater. Res. **44**, 451 (2014).
[2] A. Kusne, T. Gao, A. Mehta, L. Ke, M. Nguyen, K. Ho, V. Antropov, C. Wang, M. Kramer, C. Long *et al.*, Sci. Rep. **4**, 6367 (2014).
[3] Y. Yang, L. Kong, S. Sun, D. Gu, and B. Cheng, J. Appl. Phys. **63**, 3702 (1988).
[4] K. Buschow, J. Magn. Magn. Mater. **100**, 79 (1991).
[5] Q. Pan, Z. Liu, and Y. Yang, J. Appl. Phys. **76**, 6728 (1994).
[6] A. Sakuma, J. Phys. Soc. Jpn. **61**, 4119 (1992).
[7] W. Körner, G. Krugel, and C. Elsässer, Sci. Rep. **6**, 24686 (2016).
[8] Y. Yang, H. Sun, Z. Zhang, T. Luo, and J. Gao, Solid State Commun. **68**, 175 (1988).
[9] J. Franse and R. Radwański, *Handbook of Magnetic Materials* (Elsevier, Amsterdam, 1993), Vol. 7, Chap. 5, pp. 307–501.
[10] H. Li and J. Coey, *Handbook of Magnetic Materials* (Elsevier, Amsterdam, 1991), Vol. 6, Chap. 1, pp. 1–83.
[11] B. Hu, H. Li, and J. Coey, J. Appl. Phys. **67**, 4838 (1990).
[12] J. Coey, J. Magn. Magn. Mater. **80**, 9 (1989).
[13] F. De Boer, Y. Huang, D. De Mooij, and K. Buschow, J. Less-Common Met. **135**, 199 (1987).
[14] M. Solzi, L. Pareti, O. Moze, and W. David, J. Appl. Phys. **64**, 5084 (1988).
[15] O. Isnard, S. Miraglia, M. Guillot, and D. Fruchart, J. Alloys Compd. **275-277**, 637 (1998).
[16] I. Tereshina, P. Gaczyski, V. Rusakov, H. Drulis, S. Nikitin, W. Suski, N. Tristan, and T. Palewski, J. Phys. Condens. Matter **13**, 8161 (2001).
[17] C. Zhou, F. Pinkerton, and J. Herbst, J. Appl. Phys. **115**, 17C716 (2014).
[18] K. Ohashi, H. Ido, K. Konno, and Y. Yoneda, J. Appl. Phys. **70**, 5986 (1991).
[19] J. Wang, N. Tang, B. Fuquan, W. Wang, W. Wang, G. Wu, and F. Yang, J. Phys. Condens. Matter **13**, 1617 (2001).
[20] V. Sinha, S. Cheng, W. Wallace, and S. Sankar, J. Magn. Magn. Mater. **81**, 227 (1989).
[21] S. Cheng, V. Sinha, B. Ma, S. Sankar, and W. Wallace, J. Appl. Phys. **69**, 5605 (1991).
[22] O. Moze, L. Pareti, and K. Buschow, J. Phys. Condens. Matter **7**, 9255 (1995).
[23] J. Wang, B. Fuquan, C. Yang, and F. Yang, J. Magn. Soc. Jpn. **23**, 459 (1999).
[24] Y. Yang, X. Zhang, L. Kong, Q. Pan, and S. Ge, Appl. Phys. Lett. **58**, 2042 (1991).
[25] Y. Yang, X. Zhang, L. Kong, Q. Pan, S. Ge, J. Yang, Y. Ding, B. Zhang, C. Ye, and L. Jin, Solid State Commun. **78**, 313 (1991).
[26] D. Hurley and J. Coey, J. Phys. Condens. Matter **4**, 5573 (1992).
[27] Q. Qi, Y. Li, and J. Coey, J. Phys. Condens. Matter **4**, 8209 (1992).
[28] Z. Li, X. Zhou, and A. Morrish, J. Phys. Condens. Matter **5**, 3027 (1993).
[29] S. Nikitin, I. Tereshina, V. Verbetsky, and A. Salamova, Intl. J. Hydrogen Energy **24**, 217 (1999).
[30] S. Nikitin, I. Tereshina, V. Verbetsky, and A. Salamova, J. Alloys Compd. **316**, 46 (2001).
[31] D. Zhang, Z. Zhang, Y. Chuang, B. Zhang, J. Yang, and H. Du, J. Phys. Condens. Matter **7**, 2587 (1995).
[32] J. Coey, J. Allan, A. Minakov, and Y. Bugaslavsky, J. Appl. Phys. **73**, 5430 (1993).
[33] J. Chaboy, A. Marcelli, L. Bozukov, F. Baudelet, E. Dartyge, A. Fontaine, and S. Pizzini, Phys. Rev. B **51**, 9005 (1995).
[34] L. Nordström, O. Eriksson, M. Brooks, and B. Johansson, Phys. Rev. B **41**, 9111 (1990).
[35] O. Eriksson, L. Nordström, M. Brooks, and B. Johansson, Phys. Rev. Lett. **60**, 2523 (1988).
[36] A. Alam, M. Khan, R. W. McCallum, and D. D. Johnson, Appl. Phys. Lett. **102**, 042402 (2013).
[37] Y. Wang, J. Shen, N. Chen, and J. Wang, J. Alloys Compd. **319**, 62 (2001).
[38] L. Ke, D. Kukusta, R. W. Mccallum, and V. Antropov, in *IEEE Magnetics Conference (INTERMAG)* (IEEE, New York, 2015).
[39] Z. Li, X. Zhou, and A. Morrish, J. Appl. Phys. **69**, 5602 (1991).
[40] J. Liang, Q. Huang, A. Santoro, J. Wang, and F. Yang, J. Appl. Phys. **86**, 2155 (1999).
[41] O. Andersen, Phys. Rev. B **12**, 3060 (1975).
[42] M. Methfessel, M. van Schilfgaarde, and R. A. Casali, in *Lecture Notes in Physics*, edited by H. Dreysse (Springer-Verlag, Berlin, 2000), Vol. 535.
[43] A. Mackintosh and O. Andersen, *Electrons at the Fermi Surface* (Cambridge University Press, Cambridge, England, 1980).
[44] V. Antropov, L. Ke, and D. Åberg, Solid State Commun. **194**, 35 (2014).
[45] L. Ke and M. van Schilfgaarde, Phys. Rev. B **92**, 014423 (2015).
[46] L. Ke, K. Belashchenko, M. van Schilfgaarde, T. Kotani, and V. Antropov, Phys. Rev. B **88**, 024404 (2013).
[47] L. Ke, M. van Schilfgaarde, and V. Antropov, Phys. Rev. B **86**, 020402 (2012).
[48] U. von Barth and L. Hedin, J. Phys. C **5**, 1629 (1972).

[49] P. Haas, F. Tran, and P. Blaha, Phys. Rev. B **79**, 085104 (2009).
[50] G. Kresse and J. Hafner, Phys. Rev. B **47**, 558 (1993).
[51] G. Kresse and J. Furthmüller, Phys. Rev. B **54**, 11169 (1996).
[52] G. Kresse and D. Joubert, Phys. Rev. B **59**, 1758 (1999).
[53] S. Obbade, D. Fruchart, M. Bououdina, S. Miraglia, J. L. Soubeyroux, and O. Isnard, J. Alloys Compd. **253**, 298 (1997).
[54] O. Moze, L. Pareti, M. Solzi, and W. David, Solid State Commun. **66**, 465 (1988).
[55] D. Goll, R. Loeffler, R. Stein, U. Pflanz, S. Goeb, R. Karimi, and G. Schneide, Phys. Status Solidi (RRL) **8**, 862 (2014).
[56] X. Zhao, M. Nguyen, W. Zhang, C. Wang, M. Kramer, D. Sellmyer, X. Li, F. Zhang, L. Ke, V. Antropov *et al.* Phys. Rev. Lett. **112**, 045502 (2014).
[57] J. Trygg, B. Johansson, and M. Brooks, J. Magn. Magn. Mater. **104**, 1447 (1992).
[58] B. Hu, H. Li, J. Gavigan, and J. Coey, J. Phys. Condens. Matter **1**, 755 (1989).
[59] N. Thuy, J. Franse, N. Hong, and T. Hien, J. Phys. Colloques **49**, 499 (1988).
[60] E. Tereshina, I. Telegina, T. Palewski, K. Skokov, I. Tereshina, L. Folcik, and H. Drulis, J. Alloys Compd. **404**, 208 (2005).